Supplementary Materials for

Early life stress confers lifelong stress susceptibility in mice via ventral tegmental area OTX2

Catherine J. Peña, Hope G. Kronman, Deena M. Walker, Hannah M. Cates, Rosemary C. Bagot, Immanuel Purushothaman, Orna Issler, Yong-Hwee Eddie Loh, Tin Leong, Drew D. Kiraly, Emma Goodman, Rachel L. Neve, Li Shen, Eric J. Nestler*

*Corresponding author. Email: eric.nestler@mssm.edu

Published 16 June 2017, *Science* **356**, 1185 (2017)
DOI: 10.1126/science.aan4491

This PDF file includes

Other Supplementary Materials for this manuscript include the following:
(available at www.sciencemag.org/cgi/content/full/science.aan4491/DC1)

Materials and Methods

Mice

C57BL/6J mice were maintained on a 12 h light/dark cycle (lights on at 7 am) with *ad libitum* access to food and water. All experiments were conducted in accordance with the guidelines of the Institutional Animal Care and Use Committee at Mount Sinai and of the Society for Neuroscience. All behavioral testing occurred during the animals' light cycle. Experimenters were blind to experimental group, and order of testing was counterbalanced during behavioral experiments. All testing was performed with male mice.

Generation of litters: Two C57BL/6J females (Jackson) were mated with one male in our animal facility. The male was removed after one week and the females separated into individual cages 1-3 days prior to giving birth. Litters were weighed and counted and cages cleaned on the day of birth (PND0) but otherwise undisturbed. Cages were cleaned with minimal disruption to the litter once/week. Offspring were weaned at postnatal PND21 with males and females weaned separately into cages of 3-5 mice, keeping littermates together and only combining pups from different litters and of the same experimental condition to maintain 3 or more mice/cage.

Early Life Stress

The early life stress paradigm was adapted from established rat paradigms of maternal separation for 2-4 hours/day (*10*), and disordered maternal care induced by limited homecage bedding material (*11*). Two postnatal pre-weaning windows of stress were tested based on timing of typical maternal separation, sensitive windows of rat maternal care (*22*, *23*), and on evidence for a stress hyporesponsive period prior to PND10 in rodents (*12*). Early postnatal stress was thus administered for 10 days from PND2-12; late postnatal stress was administered for either 10 or 7 days, from PND10-20 (initial cohorts for behavior and RNA-seq) or PND10-17 (subsequent cohorts, after further piloting that both 7 and 10 day protocols produced indistinguishable effects, used for gene expression time-course, immunohistochemistry, viral manipulation, and ChIP). Postnatal stress consisted of limiting nesting material (Enviro-Dri) to 1/3 amount given to standard-reared (Std) litters, and maternal separation in which whole litters were moved to clean cages for 4 hours/day. Body temperature of pups <PND14 was maintained by placing cages on heating pads on the lowest setting. Temperature of PND2-7 pups huddled in the homecage nest ranged from 28.6-33.2ºC, depending on presence of dam and age, and temperature of separated pups ranged from 27.3-30.5ºC. Nesting material was restored to litters on the final day of postnatal stress.

Overall condition of mice and body weight: Offspring survival was not affected by early or late postnatal stress. There were no observable differences in coat condition or barbering behavior. No differences in gross locomotor behavior or water drinking were detectable during testing. Mice were weighed at birth, PND7, PND21, PND45, and PND65. Weights of mice <PND21 are an average of all pups in a litter.

Adult Social Defeat Stress and Behavioral Testing

Social defeat: Experiments utilized an established chronic social defeat stress protocol to induce depressive-like behaviors in male mice (*13*, *24*). Retired breeder CD1 male mice (Charles River) were screened for aggressiveness. As described by Bagot et al (2016), adult (PND60-70) C57BL/6J mice were subjected to 10 daily, 5-min defeats by a novel CD1 aggressor mouse and were then housed across a plexiglass divider to allow for sensory contact for the remainder of the

day. C57BL/6J experimental mice were counterbalanced by early life condition and viral manipulation so that each group was rotated through overlapping sets of the same aggressor mice. Attack latency, duration, and frequency were not different among groups. Control mice were housed in cages separated from other control mice by a plexiglass divider and were rotated to a different cage daily.

An accelerated social defeat paradigm (twice daily defeats for 5 d for 10 total defeats) was utilized after adult *Otx2* overexpression to capture behavior within the timeframe of HSV expression (*13*). A sub-threshold social defeat procedure (once daily defeats for 5 days) which does not reduce social interaction or sucrose preference in standard mice (*13*) was utilized with *Otx2* knockdown to test enhanced vulnerability to stress.

Timing of behavioral testing: Mice were single-housed on the last day of defeat and through behavioral testing *(11)* until euthanasia. All behavioral tests were performed during the light cycle. Social avoidance was tested on the day following the final defeat and two-bottle sucrose choice began immediately upon return to the home cage. In the cohort for which open field and forced swim behavior was measured and for which RNA-sequencing was performed, the behaviors were measured the following day in the morning and afternoon, respectively. All mice were killed the morning after the last behavioral test. All behavioral data presented in Fig. 1 are from a single cohort for which RNA-sequencing was performed, with the exception of sucrose preference for which data was incomplete for the initial cohort and data from a validation cohort is also included. Group sizes for all experiments are presented in Table S2.

Social avoidance testing: Social avoidance behavior was assessed with a novel CD1 mouse in a two-stage social-interaction test under red lighting (*25*). In the first 2.5-min test (no target), the experimental mouse was allowed to freely explore an arena (44×44 cm) containing a plexiglass and wire mesh enclosure (10×6 cm) centered against one wall of the arena. In the second 2.5 min test (target), the experimental mouse was immediately returned to the arena with a novel CD1 mouse enclosed in the plexiglass wire mesh cage. Time spent in the 'interaction zone' (14×26 cm) surrounding the plexiglass wire mesh cage, 'corner zones' (10×10 cm), and 'distance travelled' within the arena was measured by video tracking software (Ethovision, Noldus). Visualization of social interaction behavior in heatmaps is presented as the mean time spent in an area of the arena for the entire group, with warmer colors indicating more time in a location (Ethovision, Noldus). A social interaction ratio (SI Ratio) was calculated as time spent exploring the interaction zone with the target present divided by time spent exploring the interaction zone with target absent. Accelerated and sub-threshold social defeat followed a similar protocol altered as described above. Susceptibility and resilience were defined as having an SI Ratio of <0.9 or >1.1, respectively, with remaining mice characterized as "indifferent." The effects of P2-12 or P10-17/20 stress on social avoidance behavior after adult social defeat have been replicated in three cohorts, with additional replication of the P10-17 stress effect such as during viral manipulation.

Anhedonia: Sucrose preference, a measure of anhedonia-like behavior in mice, was assessed in a two-bottle choice test (*13*). Mice were acclimated overnight with two bottles of drinking water (50-mL conical tubes fitted with spouted rubber tops). After social interaction testing, water in one bottle was replaced with a 1% sucrose solution and both bottles weighed. Bottles were weighed again daily at the beginning of the light cycle for two days. Bottle locations were switched at each measurement to prevent location habituation. Percent sucrose preference was calculated as amount (g) sucrose solution consumed over total amount (g) of water and sucrose consumed.

A *"composite depression score"* was calculated based on all tests of depression-like behavior. For the initial behavioral cohort (Fig1 and figS1), the behaviors included social interaction ratio, sucrose preference, and forced swim immobility. For viral manipulation cohorts (Fig. 3 and fig. S3), the behaviors included social interaction ratio and sucrose preference. Depression-like behavior was considered as SI Ratio <1, sucrose preference < mean of all control mice, and forced swim immobility > mean of all control mice. A percent of tests on which each mouse met depression-like criteria was then calculated.

Open field test: Exploration of an open field arena (44×44 cm) was assessed during a 10 min test under red lighting. A video-tracking system (Ethovision, Noldus) measured locomotor activity, as well as the time spent in the center (34×34 cm) and periphery of the test arena as an index of anxiety. For the *forced swim test*, mice were individually placed in beakers of 25°C water for 6 min with ambient lighting. Immobility was assessed by a video-tracking system as a measure of depression-like behavior (Ethovision, Noldus).

Immunohistochemistry, Imaging, and Cell Counting

PND17 or PND60 males were terminally anesthetized with ketamine/xylazine and transcardially perfused with PBS followed by 4% paraformaldehyde, and brains were postfixed overnight in 4% paraformaldehyde at 4ºC. Brains were then dehydrated in 30% sucrose at 4°C until isotonic and stored at -80°C. Coronal sections (40 μm) were sliced on a freezing microtome and washed 3x with PBS and blocked with normal donkey serum at room temperature for 1 h in PBS with 0.2% Triton-X (PBST). Sections were then incubated in primary antibodies overnight at 4°C (see Table S4) in PBST. Sections were then washed 3x in PBST and incubated with secondary antibodies (Table S4) for 2 h at room temperature. Sections were washed in PBST, stained with hoechst (Invitrogen) in PBST for 20 min, and washed again before mounting on slides and coverslipping with ProLong Gold with Anti-fade (Invitrogen). OTX2 protein was observed in the expected locations of the brain. The specificity of the anti-OTX2 antibody (ProteinTech) was validated by immunoprecipitation of a chromatin dilution series and Western blotting of pull-down with an independent OTX2 antibody by a different manufacturer, which showed a protein of the expected size (Table S4; fig. S4).

For quantification of immunohistochemistry, slides were imaged on an Axio Observer Microscope (Zeiss) fitted with fluorescent filters. Only high-quality slices at a similar level along the A-P axis were imaged at 20x-magnification (AxioVision imaging software, Zeiss), such that 3-6 slices per mouse were imaged and quantitated (n=6-10). Analysis of cell counts and colocalization was performed using ImageJ by an observer blind to condition. Intensity thresholds were adjusted to accurately count moderate- to highly-immunoreactive (+) cells. A mean count per mouse was used for statistical evaluation. High-resolution images to determine cell type of HSV infection (fig. S2J) were taken on a Zeiss LSM710 Confocal microscope at 40X or 63X in slices obtained from an adult standard-reared male.

RNA and Chromatin Extraction

Mice were rapidly cervically dislocated directly from the home cage 1 day after the final behavioral test. Brains were rapidly removed, and bilateral 1 mm-thick 16 gauge punches of VTA were taken fresh and flash-frozen on dry ice. NAc punches were 14 gauge. Total RNA was isolated with TriZol reagent (Invitrogen) and purified with RNeasy Micro Kits (Qiagen). All RNA samples were determined to have A260/280 values ≥1.8 (Nanodrop); samples for RNA-seq had RIN values >9 (BioAnalyzer, Agilent). Samples for each RNA-seq library were pooled from

3 animals after TriZol isolation. Samples for qPCR were from individual animals, and cDNA was created with a reverse-transcription kit (Applied Biosystems).

For chromatin immunoprecipitation (ChIP) procedures, bilateral VTA punches from 3 animals were pooled at the time of tissue extraction and flash-frozen on dry ice. ChIP was performed as previously described (*26*) with some updates. Samples were briefly cross-linked in 1% formaldehyde and quenched with 2 M glycine. Samples were gently homogenized in cold PBS with protease inhibitors (PIs), incubated in cold cell lysis buffer (5mM PIPES pH 8, 85mM KCl, 0.5% NP40) with PIs, and sonicated in cold nuclear lysis buffer (50mM Tris-HCl pH 8, 10mM EDTA, 1% SDS) with PIs at 4ºC for 20-25 cycles in a Bioruptor (Diagenode) until peak fragment size was 200-600 bp as assessed on a BioAnalyzer (Agilent) and samples were frozen in aliquots at -80ºC until immunoprecipitation with previously validated antibodies (*21*). Sample size was n=4-7 samples per group for qChIP, n=4 samples per group for ChIP-seq.

RNA and ChIP qPCR Data Analysis

All real-time PCR reactions were run in triplicate and used SYBR-green on a QuantStudio 7 (ThermoFisher). The 2^(-ΔΔCt) method was used to calculate RNA expression analysis compared to the standard-reared group with ß-actin (*Actb*) and *Hprt* as control genes (*27*), which were not affected by early life stress or social defeat stress. See Table S5 for primer sequences. For mRNA expression time-course, data were normalized to the PND21 standard-reared group. Several cohorts were run and adjusted to a pegged sample run with each cohort. Effects were maintained across cohort—there was not a main effect of cohort, and thus data were pooled (Fig. 2E).

Real-time ChIP-qPCR (qChIP) primers were designed in proximity to OTX2 binding motif sequences. For each gene of interest, separate primer pairs were designed to amplify either within or outside of H3K4me1-enriched regulatory regions, ascertained from VTA ChIP-seq performed. qChIP results were calculated as percent of input.

RNA-Sequencing Library Preparation

500 ng of purified RNA was used to prepare libraries for sequencing using the Truseq mRNA library prep kit (Illumina RS-122-2001/2). Briefly, the cDNA was synthesized from poly-A-selected and then fragmented total RNA using random hexamers, followed by end-repair and ligation with sequencing adaptors. The libraries were then size selected and purified using AMPure XP beads (Beckman Coulter, Brea, CA). Barcode bases (6 bp) were introduced at one end of the adaptors during PCR amplification steps. Quality and concentration of libraries were confirmed on a Bioanalyzer (Agilent) and libraries were sequenced on an Illumina Hi-seq machine with 50-bp single-end reads in the Mount Sinai Genomics Core Facilities. Samples were multiplexed to produce >30 million reads per sample. Sample size was n=4-6 independent samples per group.

RNA-Seq Data Analysis

RNA-seq differential expression analysis: RNA-seq reads were aligned to mouse genome NCBI37 (mm9) using Tophat2 (*28*). The average mapping rate was 93% (Table S6). Uniquely aligned short reads were counted using HTSeq-counts. Low and non-expressed genes with less than 5 reads in at least 80% of samples in a condition were omitted from the analysis. Principal component analysis was used to detect outliers for removal, although none were identified. Normalization and differential analysis was performed using voom-limma (*29*). Significance was

set at uncorrected $p<0.05$ for broad pattern identification. A fold-change (FC) threshold was set at >1.3. Heatmaps were generated using Multiple Experiment Viewer and gene ontology analysis was performed using DAVID Bioinformatics Resource 6.7 (*30*, *31*). Upstream regulator predictions were made using the April 2014 release and updated with the August 2016 release of Ingenuity Pathway Analysis (IPA, Qiagen) for late postnatal stress-control vs. standard reared-control comparisons. Predicted upstream regulators included were top predicted genes, made from ≥3 up- or down-regulated DEGs.

Rank-rank hypergeometric overlap (RRHO): Full differential expression lists were ranked by the -log10(p-value) multiplied by the sign of the fold change from the Cuffdiff analysis. RRHO was used to evaluate the overlap of differential expression lists between pairs of brain regions (*32-34*). A one-sided version of the test only looking for over-enrichment was used. RRHO difference maps were produced for pairs of RRHO maps (Late postnatal stress-Control vs. Standard-Control and Standard-Defeat vs. Standard-Control) by calculating for each pixel the normal approximation of difference in log odds ratio and standard error of overlap between Late postnatal stress-Control vs. Standard-Control and Standard-Defeat vs. Standard-Control. This Z score was then converted to a P-value and corrected for multiple comparisons across pixels.

Fisher's Exact test for motif analysis: The locations of the OTX2 transcription factor binding motif [GGATTA (TAATCC)] on the MM10 genome was identified using a custom-written perl script. Genes with the OTX2 motif within 1kb of the transcription start site was then tabulated, and their association with differentially expressed genes calculated using the GeneOverlap R bioconductor package (v1.8.0; (*35*)), which implements the Fisher's Exact Test to find statistical significance.

ChIP and ChIP-seq Library Preparation

Magnetic beads (Dynabeads M-280 Sheep anti-Mouse/Rabbit IgG) were blocked and incubated with antibody (see Table S4) at 4ºC for 6 h overnight. Anti-OTX2 antibody (ProteinTech) was previously validated for ChIP-seq (*21*) and confirmed in our hands at a range of chromatin input by Western bloting with standard methods (*36*) (see above). Either 500 ng (qChIP) or 1 µg (ChIP-seq; pooling 2-3 samples, or 6-9 mice) of chromatin per sample was incubated with antibody-bead mix for 6-16 h for each immunoprecipitation. Prior to antibody incubation, 5% aliquots were removed from each sample as input. Chromatin samples were then washed 1x each with low salt buffer (0.1% SDS, 1% TritonX100, 2mM EDTA pH 8, 150 mM NaCl, 20mM Tris-HCl pH 8), high salt buffer (0.1% SDS, 1% TritonX100, 2mM EDTA pH 8, 500 mM NaCl, 20mM Tris-HCl pH 8), LiCl buffer (150mM LiCl, 1% NP40, 1% NaDOC, 1mM EDTA, 10mM Tris-HCl pH 8), and TE buffer (50mM NaCl, 10mM Tris-HCl pH 8, 1mM EDTA). Samples were then eluted in buffer (1% SDS, 100mM $NaHCO_3$), and reverse-crosslinked overnight at 65ºC. After RNAse and protinase K incubations, DNA was purified using the PCR Purification Kit (Qiagen) and quality was assessed on a BioAnalyzer. Primers for qChIP were designed to amplify regions including an Otx2 binding motif (see Table S5).

ChIP-seq libraries (n=4 per group) were prepared using the entire immunoprecipitation product with the NEBNext Ultra DNA Library Prep kit for Illumina (catalogue E7370, New England BioLabs), without size selection, as recommended for low-input samples. Barcodes were used to multiplex samples to achieve >80-million reads/sample. Library size and quality was assessed on a BioAnalyzer prior to sequencing on an Illumina Hi-seq machine using V4 chemistry with 100-bp single-end reads in the Mount Sinai Genomics Core Facilities.

ChIP-Seq Data Analysis

The H3K4me1 ChIP-sequencing yielded >80 million total reads per sample (Table S6), and was first checked for quality using the various metrics generated by FastQC (v0.11.2; (*37*). Raw sequencing reads were then aligned to the mouse MM10 genome using default settings of Bowtie (v2.2.0; (*38*), where ~78% were successfully aligned. Only uniquely mapped reads were retained and the alignments were subsequently filtered using the SAMtools package (v0.1.19; (*39*) to remove duplicate reads, leaving an average of 63.5 million mapped reads per sample for subsequent analyses. The alignment data was visualized on the genome (in CPM - counts per million mapped reads) using the Integrative Genomics Viewer (IGV; (*40*) program. Peak-calling was performed using MACS (v2.1.1; (*41*) with a FDR cutoff of 0.05.

Generation of Viral Vectors

Herpes simplex virus (HSV) was chosen to transiently manipulate gene expression based on its rapid expression within 12 hours of injection, maximal expression between 2-4 days, and reduced expression thereafter, being undetectable by day 7 (*42*). Viral construction and surgery were carried out according to standardized methods (*42*, *43*). We over-expressed genes of interest using bicistronic p1005 HSV vectors expressing *Gfp* alone or *Gfp* and *Otx2* (Origene), miR-*Otx2*, or miR-*LacZ*. In this system, GFP expression is driven by a cytomegalovirus (CMV) promoter, while the gene of interest is driven by the IE4/5 promoter. Viral vector expression was confirmed *in vitro* or *in vivo* via qPCR. Knockdown constructs designed to target *Otx2* mRNA were cloned using BLOCK-iT Pol II miR RNAi kit (Invitrogen). Briefly, two artificial miRNAs oligos were designed using Invitrogen's RNAi Designer (www.invitrogen.com/rnai) to target Otx2 (1: TGCTGTATAGGTCATGGGATAGGACCGTTTTGGCCACTGACTGACGGTCCT-ATCATGACCTATA; 2: TGCTGAAACCTGGAATTTCCATGAGGGTTTTGGCCACTGAC-TGACCCTCATGGATTCCAGGTTT) and directly cloned into pcDNA6.2-GW. Mouse neuroblastoma (N2a) cells, were transfected using lipofectamine 2000 (Invitrogen) with a vector that expressed *Otx2* in addition to either one of plasmids designed to target *Otx2* or *LacZ* as negative control. The degree of *Otx2* mRNA knockdown caused by the miRNA vector was assed using qRT-PCR. The second miRNA produced the most efficient down-regulation (~90% knockdown) and was further Gateway cloned (Invitrogen) into the p1005 vector used for HSV production. HSVs were confirmed to infect dopaminergic (majority) and GABAergic neurons within VTA (fig. S2J); the large majority of infected cells were dopaminergic, thus reflecting the preponderance of this cell type within this brain region.

Stereotaxic Surgery and Testing Timeline

For stereotaxic surgeries, mice were anesthetized with a mixture of ketamine (100 mg/kg) and xylazine (10 mg/kg) and positioned in a small-animal stereotaxic instrument (Kopf Instruments). The skull surface was exposed and 33-gauge syringe needles (Hamilton) were used to bilaterally infuse 0.5 µl HSV virus at a rate of 0.1 µl/min. Adult (PND60-70) VTA coordinates relative to bregma were: anterior/posterior, 3.3 mm; medial/lateral, 0.9 mm; dorsal/ventral, -4.6 mm ; 7° angle. Juvenile (PND15-17) VTA coordinates relative to bregma were: anterior/posterior, 3.2 mm; medial/lateral, 0.8 mm; dorsal/ventral, -4.5 mm; 7° angle. Needles remained lowered for 7 min to prevent backflow upon retraction. Coordinates were immunohistochemically confirmed in pilot mice to display VTA-restricted expression following surgery in separate cohorts due to the time-course of HSV expression. Spread of viruses from

injection target was limited to ±0.5 mm (fig. S2K), as documented previously for other HSVs. Juveniles were returned to their dams and littermates after recovering on a warming pad, and monitored until weaning at PND21. No qualitative differences in coat quality, grooming, gross locomotor behavior (fig. S3), or water drinking (total volume during sucrose preference testing) were detectable during testing after either juvenile or adult surgery (fig. S3A-E).

Juvenile surgery was performed at PND15-17, and adult social defeat stress was initiated at PND60-70. Adult mice underwent surgery from PND60-70 and were allowed to recover for two days after *Otx2* overexpression before entering an accelerated social defeat paradigm or control conditions. For one cohort of adult *Otx2* knockdown mice, sub-threshold social defeat was started 5 d after surgery to allow time for HSV expression and sufficient knockdown of target genes prior to adult stress, in accordance with pilot data. In the other adult *Otx2* knockdown cohort, mice recovered in standard group housing for 6 weeks prior to sub-threshold social defeat, equal to the timing after juvenile *Otx2* manipulation.

Corticosterone Assay

Submandibular blood was collected from an independent cohort of standard-reared, early, and late postnatal stressed mice at PND58-61 3 h after lights on. After three days of recovery, all mice began 10 d of social defeat. Social interaction behavior was measured on the day following the final social defeat and confirmed to be reduced only among late postnatal stress mice, and trunk blood was taken the following day 3 h after lights on. At both time points, blood was allowed to clot for 2 h at room temperature, was centrifuged at 2000xg for 20 min at 4°C, and serum was removed and stored at -20°C. Corticosterone was quantified by enzyme-linked immunosorbent assay (Parameter Corticosterone Assay KGE009, R&D Systems) according to assay instructions with the following modifications: 50 µl of serum and 50 µl of Pretreatment E were used and further diluted for a final dilution factor of 4. All samples were run in duplicate, counterbalanced across plates, and were within the standard curve.

Statistical Analysis

All statistics were performed using SPSS (PASWS, IBM, version 22.0). Outliers were defined as more than 2 standard deviations from the group mean and were removed from analysis to avoid type II error. Main effects and interactions were determined using ANOVA with Tukey's HSD post hoc analysis. Repeated-measures ANOVA was used to determine effects with multiple time points or regions sampled (behavior and genes). Two-tailed Student's *t* test was used for single comparisons among standard and late postnatally stressed mice when only two groups were generated or as indicated. Differences in proportions were tested using Kruskal-Walis non-parametric test. All significance thresholds were set at $p \leq 0.05$.

Supplementary Text

Author Contributions and Disclosures

CJP and EJN designed the research. CJP, HGK, DMW, HMC, RCB, OI, DDK, TL, and EG performed experiments. CJP analyzed the data and constructed the figures. CJP, IP, Y-HEL, and LS analyzed the sequencing data. CJP and EJN wrote the manuscript.

Extended Acknowledgements

We gratefully acknowledge Ezekiell Mouzon, Marie Doyle, and Nicolle Strat for their general laboratory assistance, many other colleagues for their fruitful discussions, and Maria Nazario for her support.

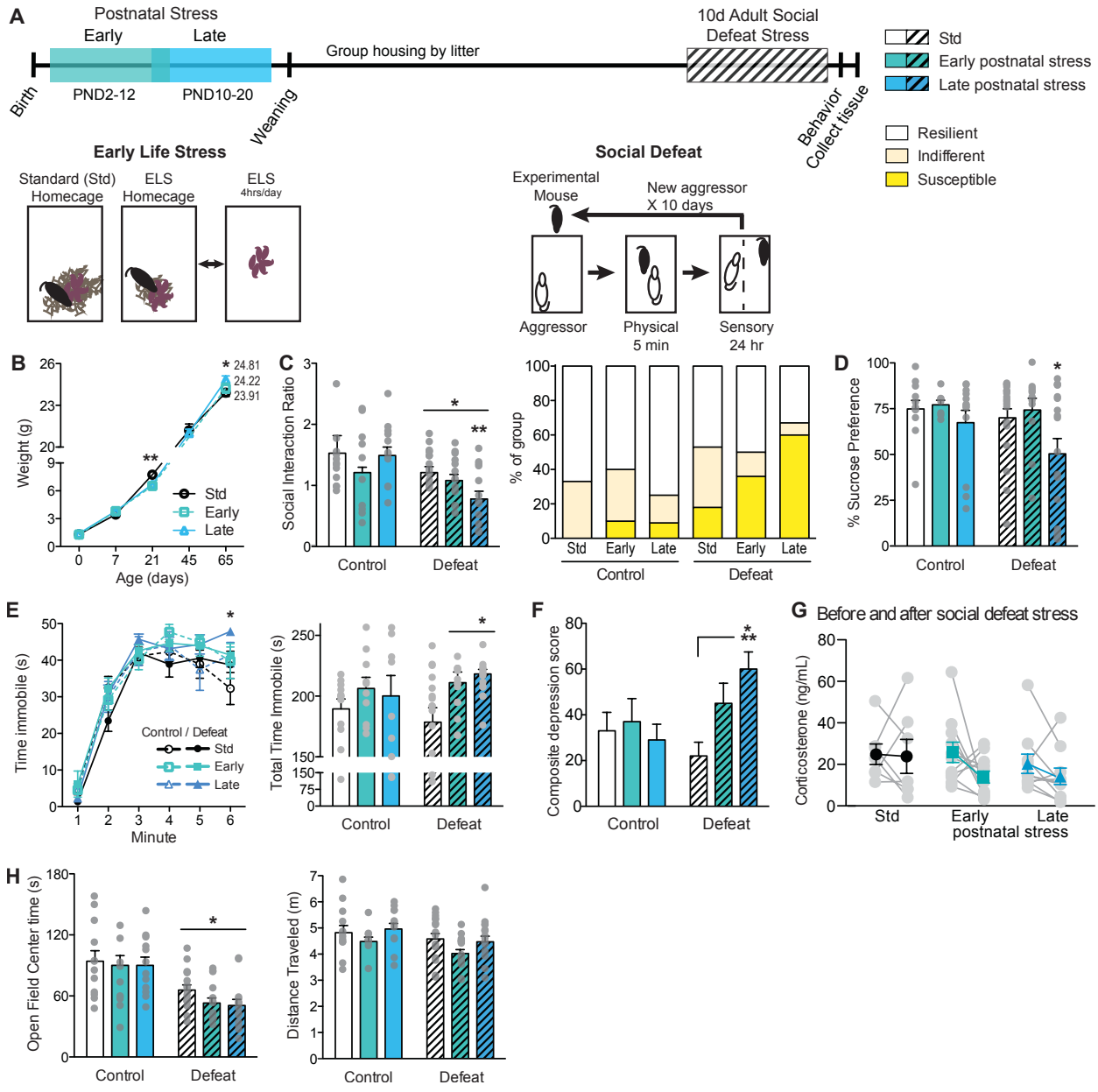

Fig. S1. Early postnatal stress does not enhance susceptibility to adult social defeat.

(**A**) Schematic timeline and behavioral paradigm in mice. (**B**) At PND21 Early and Late postnatal stress decreased weaning weight compared to standard-reared (Std) [main effect of postnatal group, $F(2,47)=11.3$, $p<0.001$, n=10-20; Tukey's HSD $p<0.001$ for both Early and Late vs. Std]. At PND65 Late, but not Early postnatal stress increased weight [$p=0.04$; n=14-16; values are shown]. (**C**) Social interaction ratio (left) and proportions of susceptible, indifferent, and resilient individuals in each group (right). There was a main effect of social defeat (Defeat) on social interaction ratio [$F(1, 58)=6.37$, $p=0.014$]. Among defeated mice, social interaction ratio was reduced among Late vs. Std mice (post-hoc $p=0.005$). (**D**) There was a main effect of postnatal stress on percent preference for 1% sucrose solution in a 2-bottle choice test [$F(2, 76)=3.19$, $p=0.047$] with a significant decrease in preference by Late stress (post hoc, $p=0.028$).

(**E**) Time immobile in a forced swim test at each min (left) and total (right). There was a main effect of postnatal stress on total immobility [$F(2, 58)=3.35$, $p=0.04$] and among defeated mice, both Early and Late stress increased immobility compared to Std (post hoc $p<0.05$). (**F**) There was an interaction between postnatal group and Defeat [$F(2,74)=4.03$, $p=0.021$] on a composite depression score, which was specifically increased among Late vs. Std defeated mice (post-hoc $p<0.001$). (**G**) Basal corticosterone was measured within mice before and after social defeat. There was a trend for defeat to lower corticosterone among Early postnatal stress mice (paired t-test, $p=0.10$). (**H**) There was a main effect of Defeat on anxiety-like behavior in the center of an open field [left; $F(1, 58)=18.75$, $p<0.001$] but no further effect of Early or Late postnatal stress. Overall activity and exploration were not altered (total distance traveled, right). Bars graphs show mean and SEM overlaid with individual data points. Bars show mean ±SEM overlaid with individual data points; *$p<0.05$, **$p<0.01$, ***$p<0.001$, bars indicate a main effect, as described.

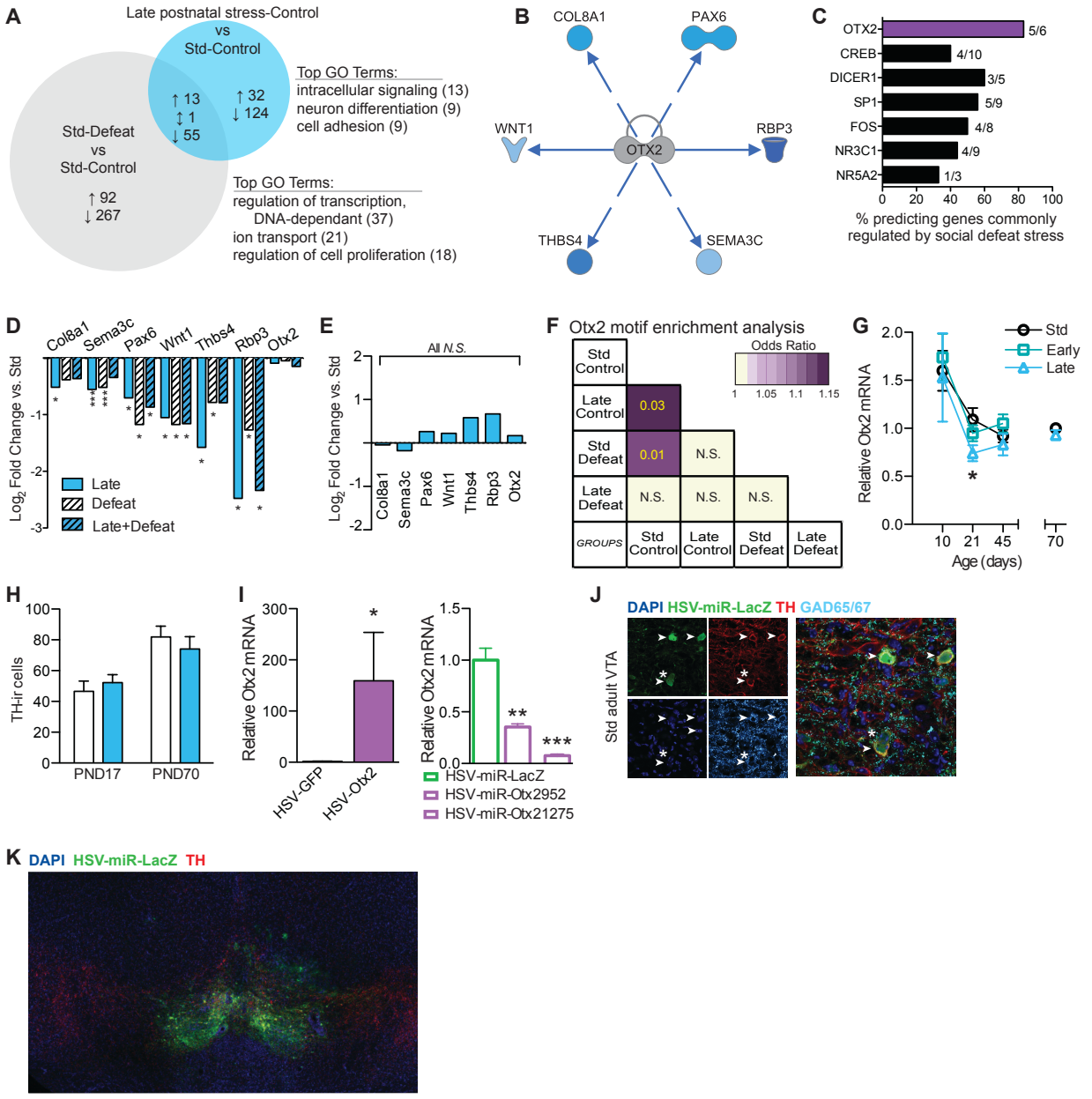

Fig. S2. Additional analysis of RNA-seq and OTX2 as an upstream regulator.

(**A**) Differentially expressed genes (DEGs; $p<0.05$) and the top associated gene ontology (GO) terms among each indicated comparison. (**B**) Network of genes contributing to prediction of OTX2 as an upstream regulator of late postnatal stress (Late)-induced transcriptional changes in VTA: color indicates direction and degree of transcriptional change. (**C**) Among top predicted upstream regulators of Late DEGs, OTX2 shares the greatest proportion on contributing genes in common with Defeat DEGs. (**D**) Fold-change vs. Std-Control in expression of OTX2-predicting genes from RNA-seq shows common expression changes after Late postnatal, Defeat, or both stresses. (**E**) Within the NAc, the major target of VTA projections, none of the OTX2-predicting genes were differentially expressed. (**F**) Fisher's Exact statistical comparison of genes significantly regulated within the indicated comparison, and genes with an OTX2 binding motif

within the promoter region: color indicates degree of enrichment; value is degree of significance. (**G**) Relative *Otx2* mRNA in you Std, Early, and Late VTA across postnatal development (PND10 n=4-5; PND21 n=11-18, p=0.031 Late vs. Std; PND45 n=5-19; PND70 time point from RNA-seq). (**H**) Count of dopamine neuron (tyrosine hydroxylase-immunoreactive) cell bodies within VTA of Std (white) and Late postnatal stress (blue) mice (PND17 n=6; PND70 n=7-10). (**I**) Validation in N2a cells of vectors to over-express (left) or knock-down (right) *Otx2* mRNA. Two miR-*Otx2* knockdown vectors were designed and tested and the vector with greatest efficiency was packaged into HSV. (**J**) HSV infects both dopamine (TH+, arrow) and GABA (GAD65/67+, star) neurons of VTA. (**K**) Representative image of viral targeting of VTA in an adult male mouse 3d after viral infection into VTA. *p<0.05, **p<0.01, ***p<0.001 compared to control.

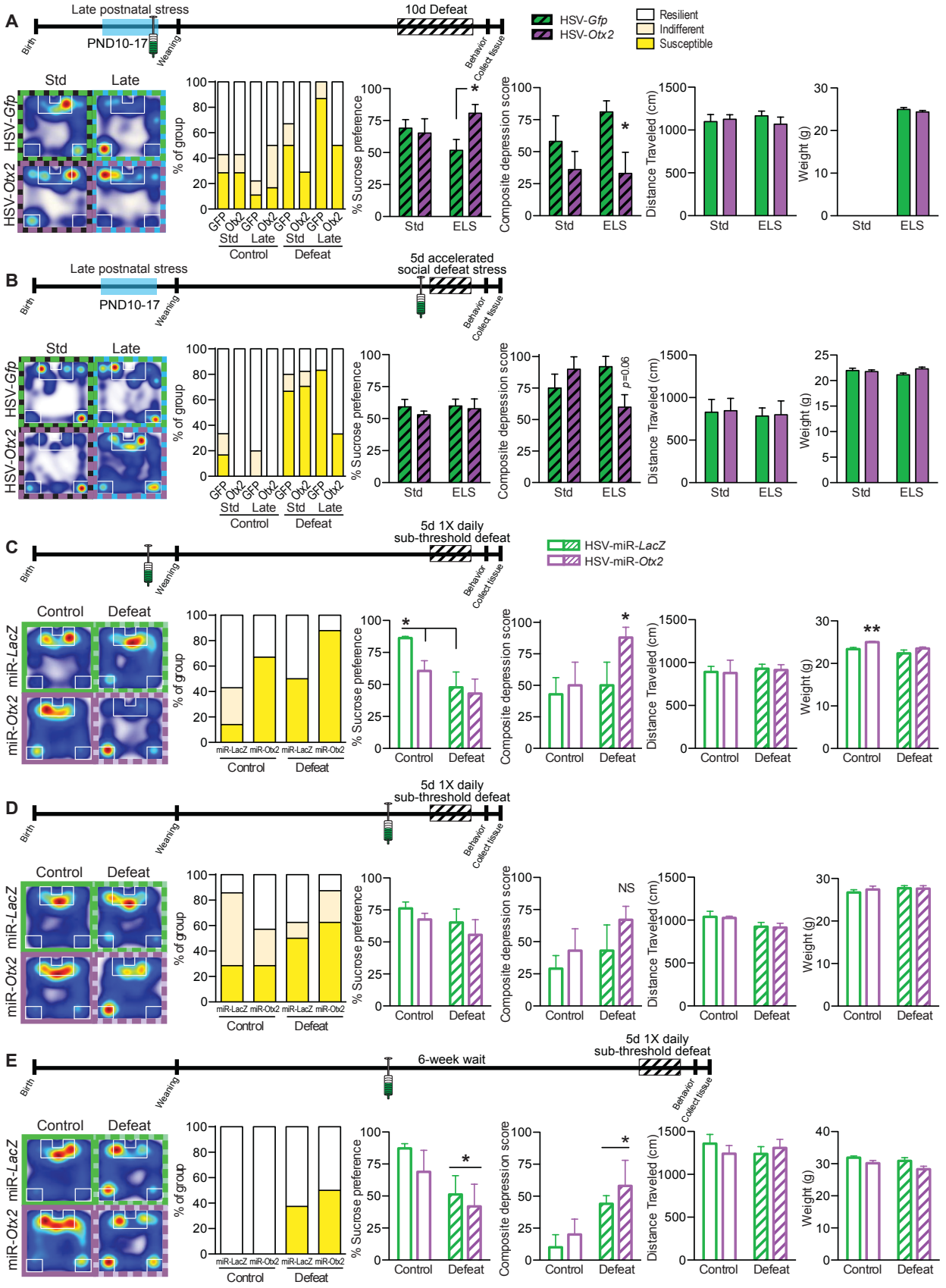
A
Late postnatal stress
PND10-17
Birth
Weaning
10d Defeat
Behavior
Collect tissue
HSV-Gfp
HSV-Otx2
Resilient
Indifferent
Susceptible
Std
Late
HSV-Gfp
HSV-Otx2
% of group
GFP
Otx2
Std
Late
Control
Defeat
% Sucrose preference
Composite depression score
Distance Traveled (cm)
Weight (g)
Std
ELS
B
Late postnatal stress
PND10-17
5d accelerated
social defeat stress
p=0.06
C
5d 1X daily
sub-threshold defeat
HSV-miR-LacZ
HSV-miR-Otx2
Control
Defeat
miR-LacZ
miR-Otx2
miR-LacZ
miR-Otx2
D
5d 1X daily
sub-threshold defeat
NS
E
6-week wait
5d 1X daily
sub-threshold defeat

Fig. S3. Additional behavioral characterization after VTA *Otx2* manipulations.

Behavior and weight after overexpression (**A**, **B**) or knockdown (**C**, **D**, **E**) of *Otx2* in VTA. Top diagrams indicate timing of postnatal stress, HSV manipulation, adult social defeat, and behavior testing. *First panel:* Heatmaps of average mouse exploration during social interaction testing with social target present. *Second panel:* Proportions of susceptible, indifferent, and resilient mice in each group. *Third panel:* Percent preference for 1% sucrose solution in a 2-bottle choice test. *Fourth panel:* Composite "depression" score. *Fifth panel:* Total distance traveled during social interaction testing with social target absent. *Sixth panel:* Mouse body weight measured either 1-3 d before (solid/open bars) or 1-2 d after (hashed bars) adult social defeat indicate that *Otx2* manipulation during the juvenile period rescues (A) or recapitulates ($p<0.01$) (C) the effects of late postnatal stress. Data are incomplete for standard-reared (Std) juvenile overexpression group in A. Bars are mean ±SEM with *$p<0.05$, **$p<0.01$ compared to control vector within condition; horizontal bars indicates a main effect of condition (ANOVA; see Table S3 for statistics).

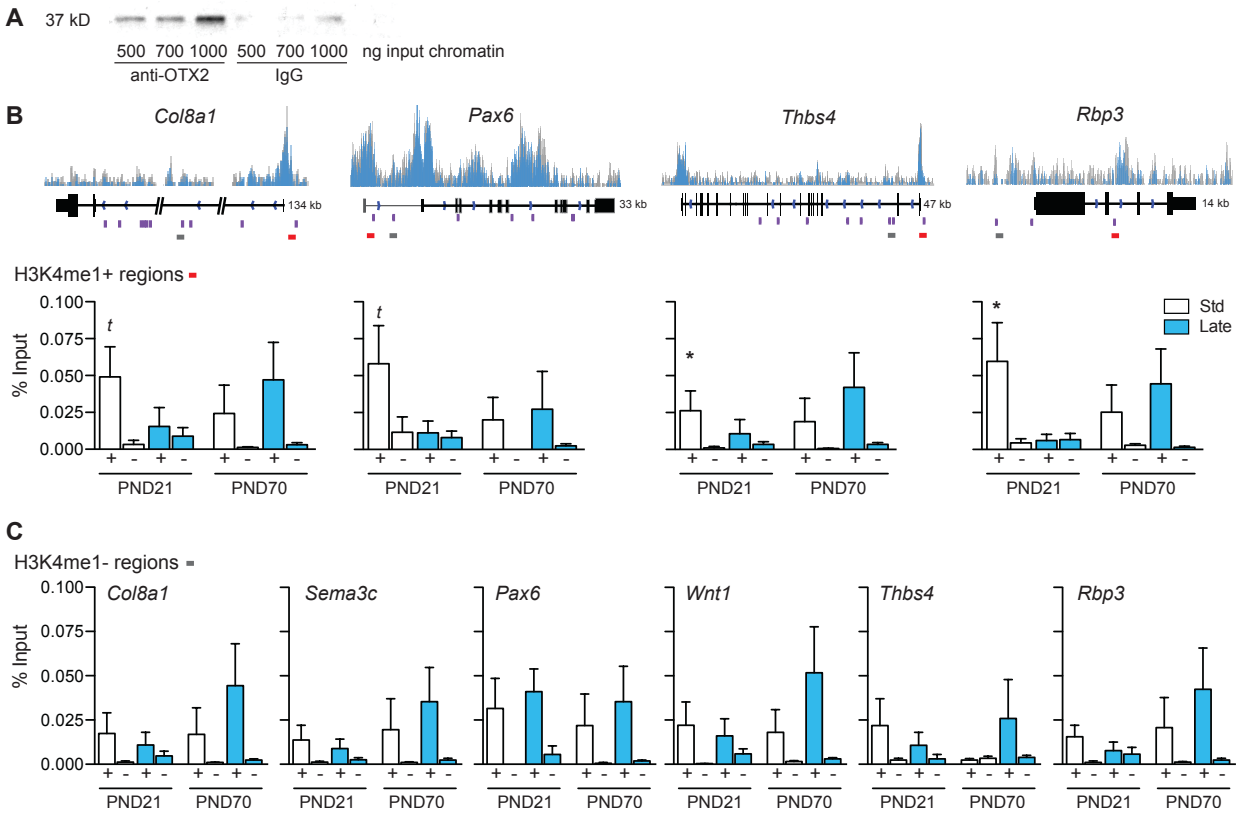

Fig. S4. OTX2 binding in H3K4me1-enriched and -depleted regions.

(**A**) Western blot validating effective OTX2 immunoprecipitation at the expected size with varying concentrations of chromatin and limited immunoprecipitation by IgG. (**B**) ChIP for OTX2 (+) and IgG (-) in VTA at PND21 and PND70 for representative OTX2 target genes after standard rearing (white/gray) or Late postnatal stress (blue). Top shows regulatory regions by H3K4me1 ChIP-seq enrichment above gene features. OTX2 binding motif sites (purple), and primer pairs for qChIP amplification are indicated (red bar: within H3K4me1+ region corresponding to bar graphs immediately below and Fig. 4; grey bar: H3K4me1- regions corresponding to **C**). (**C**) OTX2 ChIP and amplification within H3K4me1- regions. Bars (mean ±SEM) represent immunoprecipitation as percent of input (n=4-6) with $t<0.1$ and $*p<0.05$ by ANOVA with Tukey HSD post-hoc relative to IgG.

Table S1 (separate Excel file). Common differentially expressed genes.

Subset of genes differentially expressed by both early life stress (PND10-20) and adult social defeat stress.

Table S2. Group sizes and notes.

		Control			Defeat			
Experiment	**Figure**	**Standard**	**Early Stress**	**Late Stress**	**Standard**	**Early Stress**	**Late Stress**	**Notes**
Social Interaction Ratio	1A, S1C	12	10	12	17	14	15	
% Susceptible	1C, S1C	12	10	12	17	14	15	
Sucrose Preference	1D, S1D	13	7	12	19	11	20	α
Forced Swim Immobility	1E, S1E	12	10	10	14	14	10	β
Open Field Center Time	1F, S1H	12	10	12	15	14	15	β
Composite Depression Score	S1F	12	10	12	17	14	15	
Weight	S1B	9-20	9-18	9-20				γ
Corticosterone	S1G	7	11	10	7	11	10	
RNA-sequencing	2, S2	4		4	6		6	
Otx2 time course	2E, S2E	12-19	5-7	5-14				δ
PND17 IHC	2F-G	6	6					
PND70 IHC	2F-G	10	7					
H3K4me1 ChIP-seq	4, S4	4	4					
PND21 OTX2 qChIP	4, S4	6	5					
PND70 OTX2 qChIP	4, S4	5	4					

		Control		Defeat	
		Standard	**Late Stress**	**Standard**	**Late Stress**
Experiment	**Figure**	**Control, Otx2**	**Control, Otx2**	**Control, Otx2**	**Control, Otx2**
Juvenile Otx2 over-expression	2A, S2A	7,7	9,6	6,7	8,6
Adult Otx2 over-expression	2B, S2B	6,4	5,4	15,16	5,6
Juvenile Otx2 knock-down	2C, S2C	7,6		6,7	
Adult Otx2 knock-down	2D, S2D	7,7		8,8	
Adult Otx2 knock-down + 6-week wait	2E, S2E	5,5		8,6	

Notes

α 2 cohorts included

β Some animals excluded for recording issues

γ replication cohorts included at PND21 and PND65

δ replication cohorts combined

Table S3. Statistical analysis after viral manipulation.

Figure 3 / S3	Measure	Effect	Statistic	Effect	Statistic
A	Social interaction ratio	Interaction: Defeat X ELS	F(1,48)=6.682, p=0.013	Interaction: Defeat X OE	F(1,48)=5.336,p=0.025
Juvenile		Effect of OE among ELS-Defeat	T(1,12)=2.42, p=0.032	Effect of ELS among GFP-Defeat	T(1,12)=2.22, p=0.047
overexpression				Trend of OE among Std-Defeat	T(1,11)=1.98, p=0.074
	Sucrose preference	Interaction: ELS X OE	F(1,23)=3.31, p=0.081	Effect of OE among ELS-Defeat	T(1,12)=2.38, p=0.035
	Composite Depression Score	Among ELS-Defeat, effect of OE	T(1,13)=2.58, p=0.023	Among Defeat, Main effect of OE	F(1,24)=5.32, p=0.030
B	Social interaction ratio	Main effect of Defeat	F(1,34)=19.1, *p<0.001*	Interaction: OE X ELS	F(1,34)=5.23,p=0.029
Adult		Among ELS-Defeat, effect of OE	T(1,9)=2.44, p=0.050		
overexpression	Composite Depression Score	Interaction/ Defeat: ELS X OE	F(1,18)=5.35, p=0.032		
C	Social interaction ratio	Effect of KD among Defeat	T(1,11)=2.21 ,p=0.049		
Juvenile	Sucrose preference	Main effect of Defeat	F(1,21)=7.81, p=0.011	Effect of KD among Control	T(1,10)=3.18,p=0.010
knockdown	Composite Depression Score	Among Defeat, effect of KD	T(1,12)=2.83, p=0.015		
D	Social interaction ratio	Main effect of Defeat	F(1,25)=4.57, p=0.042	Interaction: Defeat X KD, trend	F(1,25)=2.96,p=0.09
Adult		Among miR-*Otx2*, effect of Defeat	T(1,13)=2.57, p=0.023		
knockdown	Composite Depression Score				
E	Social interaction ratio	Main effect of Defeat	F(1,20)=11.13, p=0.003		
Adult	Sucrose preference	Main effect of Defeat	F(1,20)=5.06, p=0.036		
knockdown	Composite Depression Score	Main effect of Defeat	F(1,20)=9.37, p=0.006		
+ 6wk wait					

Accronym	Group
KD	Knockdown
OE	Overexpression
Std	Standard-reared
ELS	Late postnatal stress (early life stress)
Ctl	Control (no Defeat)
Defeat	Adult social defeat stress

Table S4. Antibodies used for immunohistochemistry and ChIP.

Use, target, catalogue identifier, company, concentration, and species for all antibodies.

Antibody use	Antibody target	Catalogue #	Company	Concentration	Species
ChIP/ IHC/ primary	OTX2	13497-1-AP	ProteinTech	1:200	rabbit
Western Blot	OTX2	ab21990	AbCam	1:600	rabbit
IHC/ primary	Tyrosine hydroxylase (TH)	t1299	Sigma-Aldrich	1:300	mouse
IHC/ primary	GFP	GFP-1020	Aves Labs	1:500	chicken
IHC/ primary	GAD65/67	Ab1511	Millipore	1:300	rabbit
IHC/ secondary	Alexa fluor 649-anti-mouse	715-495-150	Jackson Immuno	1:500	donkey
IHC/ secondary	Alexa fluor 488-anti-chicken	703-545-155	Jackson Immuno	1:500	donkey
IHC/ secondary	Cy3-anti-rabbit	711-165-152	Jackson Immuno	1:500	donkey
ChIP	H3K4me1	Ab8895	AbCam	3 µl/IP	rabbit, polyclonal
ChIP	H3K27Ac	07-360	Millipore	4 µl/IP	rabbit, polyclonal
ChIP	Normal rabbit IgG	CS-27295	Cell Signaling	5 µl/IP	rabbit

Table S5. Primers used for qPCR and qChIP.

Gene name, accession number, forward primer sequence, and reverse primer sequence of primer pairs used in real-time PCR amplification of mRNA (qPCR; top) and immunoprecipitated DNA (qChIP; bottom). Presence of nearby H3K4me1-enrichment is indicated for each qChIP primer pair.

Mouse qPCP Primers

Gene	Accession #	Forward-sequence	Reverse-sequence
Actin, Beta	NM_007393.2	TATTGGCAACGAGCGGTTCC	TGGCATAGAGGTCTTTACGGAT
Hprt1	J00423.1	GCAGTACAGCCCCAAAATGG	GGTCCTTTTCACCAGCAAGCT
Otx2 (trans var 2,3,x1)	NM_001286482.1	TGAGGCCTGCCAAGAAGAAG	GACAAGGGGTCAGACAGTGG
Col8a1	NM_007739.2	ACCCAGCCCCAGTGGTATTA	GCACAGCCATCACATTTAGGC
Pax6	NM_001244201.1	CACCAGACTCACCTGACACC	TCACTCCGCTGTGACTGTTC
Rbp3	NM_015745.2	CTACAACCGGCCCAATGACT	AAGTAAATTCCTCGGCGGCA
Sema3c	NM_013657.5	TGTGGAAATTTCGTCCGGGT	AAGAGCATCGTCCTTTGCCA
Thbs4	NM_011582.3	CTGTGACTCCAGCCCTTGTT	CGTCACATCTGAAACCCGGA
Wnt1	NM_021279.4	GATGGTGGGGCATCGTGAA	GATGAACGCTGTTTCTCGGC

Mouse qChIP Primers

Gene	Accession #	Forward-sequence	Reverse-sequence	H3K4me1 region
Col8a1 ChIP_1	NC_000082.6	TGCAACCAACCAAGACAGGA	CTGGTGCACTCTTTGGGGAA	no
Col8a1 ChIP_2	NC_000082.6	AAGGTCCTTTCGCTGCTGAG	TCGGTGAGCAAGGTCATTCC	yes
Pax6 ChIP_1	NC_000068.7	GCTTAGTTCGGTTCCAGGCT	CTTGCTAAGGTCACCGCTCT	no
Pax6 ChIP_2	NC_000068.7	GAGATACCCAGCCATGCTCC	GGTCTAGAGAGAGGGCGTCA	yes
Rbp3 ChIP_1	NC_000080.6	GTCTCCACCCTTCCACTTCG	GAGTAGGGGGTTGAACTGGC	no
Rbp3 ChIP_2	NC_000080.6	TGGGTCCTGGTTTTGTCCAC	GACTCCAGCTGTCAGCACTT	yes
Sema3c ChIP_1	NC_000071.6	TTCTTACCGGCTTTCCCCAC	CCCTGGGTCAGGGAGGATTA	no
Sema3c ChIP_2	NC_000071.6	GCTGAGGTCTGCAGCGATT	CATCAAAGCCTTGACTGTGGC	yes
ThBs4 ChIP_1	NC_000079.6	ACGCAGGAGTCAAAGGAAGG	GCACGCATAGATCCGTGAGA	no
Thbs4 ChIP_2	NC_000079.6	CAGAGCAGGTGATCCCGTTT	CTTGTTTCCGAGGTGTCCGA	yes
Wnt1 ChIP_1	NC_000081.6	ACAGGTTGACTCAAGGTGCC	GACAGGAGACGTCCAGAAGG	no
Wnt1 ChIP_2	NC_000081.6	CATAGCCTCCTCCACGAACC	CCATTTGCACTCTCGCACAG	yes

Table S6. Sequencing quality control measures.

Sample name, total sequenced reads, and mapping rate for uniquely mapped reads for each RNA-seq (top) and ChIP-seq (bottom) sample.

Sample	Total_Reads	Mapping_rate(%)
RNA-seq		
StdCtl1	43807016	91.7
StdCtl2	42166831	92.0
StdCtl3	38987217	95.5
StdCtl4	34993894	95.7
ELS2Ctl1	43216179	91.9
ELS2Ctl2	38020367	95.8
ELS2Ctl3	35252801	95.8
ELS2Ctl4	39272728	95.7
StdDef1	46383811	91.8
StdDef2	44092328	91.7
StdDef3	37151888	95.6
StdDef4	38242925	95.4
StdDef5	45730469	91.7
StdDef6	40042614	95.5
ELS2Def1	45743380	91.8
ELS2Def2	41994495	91.9
ELS2Def3	36377793	95.4
ELS2Def4	38203601	95.7
ELS2Def5	39773240	95.9
ELS2Def6	43674343	95.7
ChIP-seq		
K4me1_ELS5	88586250	77.7
K4me1_ELS6	116590016	77.6
K4me1_ELS7	80975442	79.1
K4me1_ELS8	82320895	80.2
K4me1_Std1	108300980	74.2
K4me1_Std2	85237344	75.8
K4me1_Std3	82564573	78.1
K4me1_Std4	83265181	78.0

RNA-seq and ChIP-seq data are available at GEO
Accession number GSE89692

References

1. M. Jonson-Reid, P. L. Kohl, B. Drake, Child and adult outcomes of chronic child maltreatment. *Pediatrics*. **129**, 839–845 (2012).
2. C. Hammen, R. Henry, S. E. Daley, Depression and sensitization to stressors among young women as a function of childhood adversity. *J Consult Clin Psychol*. **68**, 782 (2000).
3. K. S. Kendler, J. W. Kuhn, C. A. Prescott, Childhood sexual abuse, stressful life events and risk for major depression in women. *Psychol Med*. **34**, 1475–1482 (2004).
4. Z.-Y. Zhang *et al.*, Early adversity contributes to chronic stress induced depression-like behavior in adolescent male rhesus monkeys. *Behavioural Brain Research*. **306**, 154–159 (2016).
5. L. M. Williams, C. Debattista, A.-M. Duchemin, A. F. Schatzberg, C. B. Nemeroff, Childhood trauma predicts antidepressant response in adults with major depression: data from the randomized international study to predict optimized treatment for depression. *Transl Psychiatry*. **6**, e799–e799 (2016).
6. S. Cabib, S. Puglisi-Allegra, F. R. D'amato, Effects of postnatal stress on dopamine mesolimbic system responses to aversive experiences in adult life. *Brain Res*. **604**, 232–239 (1993).
7. W. G. Brake, T. Y. Zhang, J. Diorio, M. J. Meaney, A. Gratton, Influence of early postnatal rearing conditions on mesocorticolimbic dopamine and behavioural responses to psychostimulants and stressors in adult rats. *Eur J Neurosci*. **19**, 1863–1874 (2004).
8. J. L. Hanson *et al.*, Cumulative stress in childhood is associated with blunted reward-related brain activity in adulthood. *Soc Cogn Affect Neurosci* (2015), doi:10.1093/scan/nsv124.
9. S. J. Russo, E. J. Nestler, The brain reward circuitry in mood disorders. *Nat Rev Neurosci*. **14**, 609–625 (2013).
10. P. M. Plotsky, M. J. Meaney, Early, postnatal experience alters hypothalamic corticotropin-releasing factor (CRF) mRNA, median eminence CRF content and stress-induced release in adult rats. *Brain Res Mol Brain Res*. **18**, 195–200 (1993).
11. C. J. Rice, C. A. Sandman, M. R. Lenjavi, T. Z. Baram, A novel mouse model for acute and long-lasting consequences of early life stress. *Endocrinology*. **149**, 4892–4900 (2008).
12. M. Rincón-Cortés, R. M. Sullivan, Early life trauma and attachment: immediate and enduring effects on neurobehavioral and stress axis development. *Front Endocrinol (Lausanne)*. **5**, 33 (2014).
13. V. Krishnan *et al.*, Molecular Adaptations Underlying Susceptibility and Resistance to Social Defeat in Brain Reward Regions. *Cell*. **131**, 391–404 (2007).
14. E. Puelles *et al.*, Otx2 regulates the extent, identity and fate of neuronal progenitor domains in the ventral midbrain. *Development*. **131**, 2037–2048 (2004).
15. B. Vernay *et al.*, Otx2 regulates subtype specification and neurogenesis in the midbrain. *Journal of Neuroscience*. **25**, 4856–4867 (2005).
16. S. Sugiyama *et al.*, Experience-Dependent Transfer of Otx2 Homeoprotein into the Visual Cortex Activates Postnatal Plasticity. *Cell*. **134**, 508–520 (2008).
17. E. S. Lein *et al.*, Genome-wide atlas of gene expression in the adult mouse brain. *Nature*. **445**, 168–176 (2007).

18. M. Di Salvio, L. G. Di Giovannantonio, D. Omodei, D. Acampora, A. Simeone, Otx2 expression is restricted to dopaminergic neurons of the ventral tegmental area in the adult brain. *Int J Dev Biol*. **54**, 939–945 (2010).
19. T.-K. Kim *et al.*, Widespread transcription at neuronal activity-regulated enhancers. *Nature*. **465**, 182–187 (2010).
20. Roadmap Epigenomics Consortium *et al.*, Integrative analysis of 111 reference human epigenomes. *Nature*. **518**, 317–330 (2015).
21. S.-H. Yang *et al.*, Otx2 and Oct4 drive early enhancer activation during embryonic stem cell transition from naive pluripotency. *Cell Rep*. **7**, 1968–1981 (2014).
22. D. Liu *et al.*, Maternal care, hippocampal glucocorticoid receptors, and hypothalamic-pituitary-adrenal responses to stress. *Science*. **277**, 1659–1662 (1997).
23. C. J. Peña, Y. D. Neugut, F. A. Champagne, Developmental Timing of the Effects of Maternal Care on Gene Expression and Epigenetic Regulation of Hormone Receptor Levels in Female Rats. *Endocrinology* (2013), doi:10.1210/en.2013-1595.
24. O. Berton *et al.*, Essential role of BDNF in the mesolimbic dopamine pathway in social defeat stress. *Science*. **311**, 864–868 (2006).
25. S. A. Golden, H. E. Covington, O. Berton, S. J. Russo, A standardized protocol for repeated social defeat stress in mice. *Nat Protoc*. **6**, 1183–1191 (2011).
26. I. Maze *et al.*, Essential role of the histone methyltransferase G9a in cocaine-induced plasticity. *Science*. **327**, 213–216 (2010).
27. T. D. Schmittgen, K. J. Livak, Analyzing real-time PCR data by the comparative C(T) method. *Nat Protoc*. **3**, 1101–1108 (2008).
28. C. Trapnell, L. Pachter, S. L. Salzberg, TopHat: discovering splice junctions with RNA-Seq. **25**, 1105–1111 (2009).
29. C. W. Law, Y. Chen, W. Shi, G. K. Smyth, voom: Precision weights unlock linear model analysis tools for RNA-seq read counts. *Genome Biol*. **15**, R29–R29 (2014).
30. Da Wei Huang, B. T. Sherman, R. A. Lempicki, Bioinformatics enrichment tools: paths toward the comprehensive functional analysis of large gene lists. *Nucleic Acids Res*. **37**, 1–13 (2009).
31. D. W. Huang, B. T. Sherman, R. A. Lempicki, Systematic and integrative analysis of large gene lists using DAVID bioinformatics resources. *Nat Protoc*. **4**, 44–57 (2009).
32. S. B. Plaisier, R. Taschereau, J. A. Wong, T. G. Graeber, Rank-rank hypergeometric overlap: identification of statistically significant overlap between gene-expression signatures. *Nucleic Acids Res*. **38**, e169–e169 (2010).
33. J. L. Stein *et al.*, A quantitative framework to evaluate modeling of cortical development by neural stem cells. *Neuron*. **83**, 69–86 (2014).
34. R. C. Bagot *et al.*, Circuit-wide Transcriptional Profiling Reveals Brain Region-Specific Gene Networks Regulating Depression Susceptibility. *Neuron*. **90**, 969–983 (2016).
35. L. Shen, GeneOverlap: Test and visualize gene overlaps. Bioconductor package, Zenodo (2016).
36. M. E. Cahill *et al.*, Bidirectional Synaptic Structural Plasticity after Chronic Cocaine Administration Occurs through Rap1 Small GTPase Signaling. *Neuron*. **89**, 566–582 (2016).

37. S. Andrews, *FastQC: A Quality Control tool for High Throughput Sequence Data* (ed. 2010).
38. B. Langmead, C. Trapnell, M. Pop, S. L. Salzberg, Ultrafast and memory-efficient alignment of short DNA sequences to the human genome. *Genome Biol*. **10**, R25 (2009).
39. H. Li *et al.*, The Sequence Alignment/Map format and SAMtools. **25**, 2078–2079 (2009).
40. J. T. Robinson *et al.*, Integrative genomics viewer. *Nat Biotechnol*. **29**, 24–26 (2011).
41. Y. Zhang *et al.*, Model-based Analysis of ChIP-Seq (MACS). *Genome Biol*. **9**, R137–R137 (2008).
42. R. L. Neve, K. A. Neve, E. J. Nestler, W. A. Carlezon, Use of herpes virus amplicon vectors to study brain disorders. *Biotechniques*. **39**, 381–391 (2005).
43. R. D. Penrod, A. M. Wells, W. A. Carlezon, C. W. Cowan, Use of Adeno-Associated and Herpes Simplex Viral Vectors for In Vivo Neuronal Expression in Mice. *Curr Protoc Neurosci*. **73**, 4–31 (2015).